J Appl Physiol 99: 624–633, 2005.
First published March 24, 2005; doi:10.1152/japplphysiol.00748.2004.

Optical monitoring of bubble size and shape in a pulsating bubble surfactometer

Shannon L. Seurynck,[1] Nathan J. Brown,[1] Cindy W. Wu,[1] Kevin W. Germino,[2] Ellen K. Kohlmeir,[1] Edward P. Ingenito,[3] Matthew R. Glucksberg,[2] Annelise E. Barron,[1] and Mark Johnson[2]

[1]*Department of Chemical and Biological Engineering and* [2]*Department of Biomedical Engineering, Northwestern University, Evanston, Illinois; and* [3]*Respiratory Division, Brigham and Women's Hospital, Boston, Massachusetts*

Submitted 16 July 2004; accepted in final form 22 March 2005

Seurynck, Shannon L., Nathan J. Brown, Cindy W. Wu, Kevin W. Germino, Ellen K. Kohlmeir, Edward P. Ingenito, Matthew R. Glucksberg, Annelise E. Barron, and Mark Johnson. Optical monitoring of bubble size and shape in a pulsating bubble surfactometer. *J Appl Physiol* 99: 624–633, 2005. First published March 24, 2005; doi:10.1152/japplphysiol.00748.2004.—The pulsating bubble surfactometer (PBS) is often used for in vitro characterization of exogenous lung surfactant replacements and lung surfactant components. However, the commercially available PBS is not able to dynamically track bubble size and shape. The PBS therefore does not account for bubble growth or elliptical bubble shape that frequently occur during device use. More importantly, the oscillatory volume changes of the pulsating bubble are different than those assumed by the software of the commercial unit. This leads to errors in both surface area and surface tension measurements. We have modified a commercial PBS through the addition of an image-acquisition system, allowing real-time determination of bubble size and shape and hence the accurate tracking of surface area and surface tension. Compression-expansion loops obtained with the commercially available PBS software were compared with those provided by the image-analysis system for dipalmitoylphosphatidylcholine, Infasurf, and Tanaka lipids (dipalmitoylphosphatidylcholine-palmitoyloleoylphosphatidylglycerol-palmitic acid, 68:22:9) at concentrations of 0.1 and 1.0 mg/ml and at frequencies of 1 and 20 cycles/min. Whereas minimum surface tension as determined by the image-analysis system is similar to that measured by the commercially available software, the maximum surface tension and the shapes of the interfacial area-surface tension loops are quite different. Differences are attributable to bubble drift, nonsinusoidal volume changes, and variable volume excursions seen with the modified system but neglected by the original system. Image analysis reveals that the extent of loop hysteresis is greatly overestimated by the commercial device and that an apparent, rapid increase in surface tension upon film expansion seen in PBS loops is not observed with the image-analysis system. The modified PBS system reveals new dynamic characteristics of lung surfactant preparations that have not previously been reported.

surface tension; dynamic; adsorption; lipids; surfactometry; lung surfactant; dipalmitoylphosphatidylcholine

SURFACTANT REPLACEMENT THERAPY is currently used to treat respiratory distress syndrome (RDS) in premature infants and has reduced mortality rates by more than 40% (16). Costly animal-derived lung surfactant replacements are typically used for the treatment of RDS. The development of synthetic or biomimetic lung surfactant replacements could significantly reduce the cost of surfactant replacement therapy, as well as minimize the risk of immune system activation and allow easier certification of purity and safety than does animal-derived surfactant. Commercially available synthetic surfactant preparations are not as effective as the animal-derived surfactants (13, 15, 31). Hence, there is a great deal of research focused on the development of new biomimetic lung surfactant replacement preparations (36).

With recent advances in biotechnology, the generation of a nearly limitless number of candidate biomimetic lung surfactant preparations for use in surfactant replacement therapy is possible (3, 19, 25, 34, 37). With such large numbers of potential surfactant replacements, it is essential to be able to rapidly evaluate the efficacy of each sample for use in humans. Ideally, each surfactant preparation could be tested in an animal model for RDS; however, these tests are both costly and time consuming, greatly limiting the number of preparations that can be evaluated. Therefore, it is desirable to have a reliable in vitro method for rapidly screening the large pool of potential lung surfactant replacements. One instrument commonly used for in vitro testing of lung surfactant is the pulsating bubble surfactometer (PBS) (9, 18).

The PBS allows both static bubble and dynamic bubble adsorption data to be collected for a surfactant preparation (18). In particular, it allows for characterization of the behavior of surfactant preparations at 37°C and at physiological frequencies of bubble pulsation. The main components of the PBS, shown in Fig. 1, are the sample chamber, the volume displacement piston, and the pressure transducer (9). The sample solution (~25 μl) is loaded into the sample chamber, which is in contact with atmospheric pressure through a capillary tube (0.55 mm ID). A bubble is formed at the bottom of the capillary by using the volume displacement piston. The bubble is pulsed at a designated frequency, with a stroke volume of 0.4 μl. Finally, a pressure transducer is used to measure the pressure in the sample chamber, which along with knowledge of the bubble radius allows surface tension to be computed by using the Laplace equation for a sphere (9).

One drawback of the PBS is the potential for "leakage" of surfactant from the air-water interface to the surfaces of the sample chamber, which has been reported to prevent the achievement of ultralow surface tensions during compression (28). However, it has been shown that, by using a modified technique of loading the sample chamber, the leakage artifact seen in the PBS system can be largely eliminated (24).

Another potential source of error is the inability of the PBS to dynamically determine the bubble size, leading to impreci-

Address for reprint requests and other correspondence: M. Johnson, Northwestern Univ., Dept. of Biomedical Engineering, 2145 Sheridan Rd., Evanston, IL 60208 (E-mail: m-johnson2@northwestern.edu).

The costs of publication of this article were defrayed in part by the payment of page charges. The article must therefore be hereby marked "*advertisement*" in accordance with 18 U.S.C. Section 1734 solely to indicate this fact.

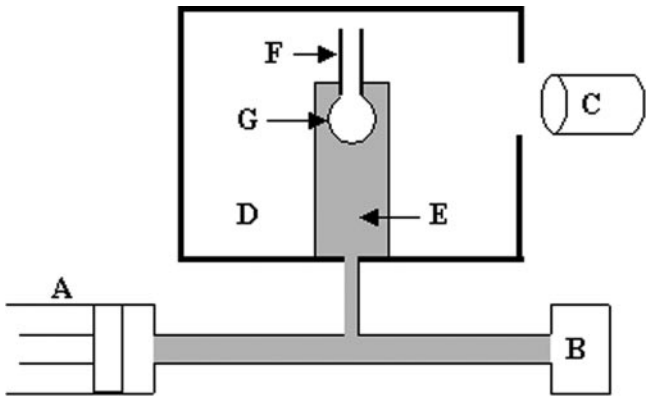

Fig. 1. Schematic diagram of the pulsating bubble surfactometer (PBS) as modified by our group. A, volume displacement piston; B, pressure transducer; C, microscope and camera; D, temperature-controlled water bath; E, sample chamber; F, capillary; G, air bubble.

sion in the dynamic determination of surface tension and bubble surface area. In addition, standard use of the PBS involves adjusting the bubble size manually throughout the run, which affects the rate of surfactant adsorption to the interface. Typical use of the PBS also relies on the assumption that the bubble shape is that of a sphere, which leads to errors at low surface tensions when the bubble is actually an ellipsoid (5, 14).

We report in this study the modification of a commercial PBS such that bubble size and shape, and therefore surface tension and interfacial area, are dynamically determined. In particular, image-acquisition capability has been added to a PBS. This system allows for more accurate characterization of the dynamic interfacial behavior of surfactant preparations. The results show that not only does this improved system give more stable results, but it also reveals new dynamic characteristics of lung surfactant preparations that have not previously been reported.

MATERIALS AND METHODS

Design of new surfactometer. We used a PBS (General Transco, Largo, FL) modified to allow the collection of real-time bubble images, therefore enabling an accurate, high-frequency determination of surface area and surface tension. A Teli CS3500 (Tokyo, Japan) monochrome video camera with 1/3-in. charge-coupled device remote video head, internal-external synchronization, and electronic shutter (1/60–1/10,000 s) was attached via a 0.50X C-mount (World Precision Instruments, Sarasota, FL). Video images were sent to a personal computer through an image-acquisition board (National Instruments, Austin, TX). An aluminum sphere (1/32 in. in diameter) was used to confirm that there is no distortion caused by the nylon cuvette and to convert pixels to units of length (mm). Using the video imaging, we are also able to detect leakage of surfactant into the capillary visually. If leakage occurs, the data can be rejected.

Two wires were pulled from the back of the PBS to transmit voltage measurements output by its pressure transducer to a National Instruments data-acquisition board. The voltage signal from the pressure transducer was converted to pressure units by calibration using a water column specially designed for use with the PBS (General Transco). Surface tension calibration was confirmed at the beginning of each day by determining the surface tension of 37°C distilled water, prefiltered through a 0.02-μm Millipore filter. The surface tension was found to be ~70 mN/m, with minimal change in surface tension upon cycling, <3 dyn/cm (data not shown).

The surface tension (γ) of the bubble was calculated by Laplace's equation (17):

$$\gamma = \frac{\Delta P}{\frac{1}{R_1} + \frac{1}{R_2}}$$

where ΔP is the pressure drop across the bubble at the location where the two radii of curvature, R_1 and R_2, are determined. Assuming the bubble to be an ellipsoid, at the side of the bubble $R_1 = b^2/a$ and $R_2 = a$ and at the apex $R_1 = R_2 = a^2/b$ (where a is the major radius and b is the minor radius of the bubble; see Fig. 2). The pressure at the apex of the bubble was corrected to account for the higher hydrostatic pressure at the bottom of the bubble due to gravity (g) by adding the product $\rho g b$ to the pressure term, where ρ is the fluid density.

The accuracy of assuming an ellipsoidal shape for the bubble was evaluated by comparing the surface tension calculated using the elliptical assumption with values determined by Graves et al. (12), who used a numerical solution to Laplace's equation for a variety of bubble shapes. The deviation in calculated surface tension, assuming an elliptical shape, was always less than or equal to 0.1 dyn/cm from the values determined for the shapes considered by Graves et al.

The surface tension is calculated at both the apex and side of the bubble, and, if the values do not agree within 10%, the data point is rejected (this is most important at low surface tensions, when the bubble is not an ellipsoid). At very low surface tensions (a few dyn/cm), the shape of the bubble was not an ellipsoid and deviated from the shapes described by Graves et al. (12).

The interfacial area (A) of the bubble is calculated for the ellipse, which is fitted to the observed bubble shape (2):

$$A = R_1^2\pi + \frac{R_2^2\pi}{\varepsilon}\ln\left(\frac{1+\varepsilon}{1-\varepsilon}\right)$$

where ϵ represents the ellipticity of the bubble [$\epsilon = (R_1^2 - R_2^2)^{1/2}/R_1$]. The area is also corrected to subtract the region where the bubble attaches to the capillary tube. Inclusion of this region in the calculation of area results in 7–12% error.

Voltage measurements from the pressure transducer and images from the camera are sent to LabVIEW acquisition boards (National Instruments) at a rate of ~10–20 times per second, and the interfacial area and surface tension of the bubble are calculated in real time. A LabVIEW program is used to find the edges of the bubble, fit the bubble shape with an ellipse, and determine the major and minor radii (see Fig. 2). The surface area and surface tension are relatively

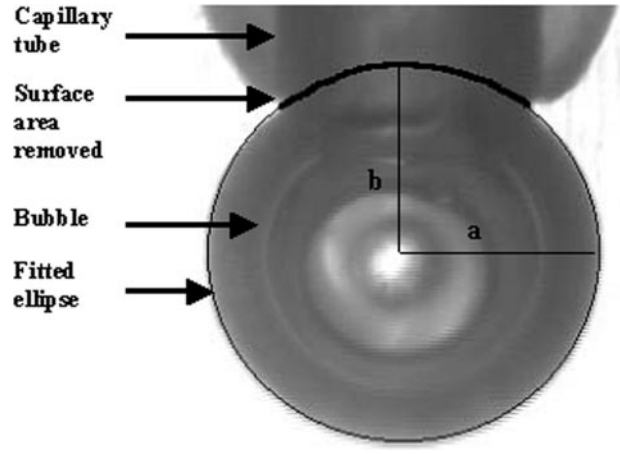

Fig. 2. Picture of bubble obtained with new imaging system during dynamic cycling. The ellipse is fit to the image at a rate of 10–20 times per second, and the surface tension and surface area are determined dynamically. *a*, Major radius; *b*, minor radius.

insensitive to small changes in the location of the edge of the bubble; a 1% error in the determination of the bubble's major or minor axis will cause an ~2% error in surface area and 1% error in surface tension.

Preparation of surfactants. Dipalmitoylphosphatidylcholine (DPPC) and palmitoyloleoylphosphatidyl-glycerol (POPG) were purchased from Avanti Polar Lipids (Alabaster, AL), palmitic acid (PA) was purchased from Aldrich (Milwaukee, WI), and Infasurf (Forest Laboratories, New York, NY) was obtained from the clinical research pharmacy at Children's Memorial Hospital (Chicago, IL). The surface activities of the different surfactants [DPPC, Infasurf, and Tanaka lipid mixture (32)] were evaluated at bulk concentrations of 0.1 and 1.0 mg/ml. In molar concentrations, DPPC was evaluated at 0.14 and 1.4 mM, and the Tanaka lipid mixture was evaluated at 0.16 and 1.6 mM. DPPC, POPG, and PA were individually dissolved to a known concentration in chloroform-methanol 3:1. The Tanaka lipid mixture, previously shown to mimic well the lipid portion of lung surfactant (32), was prepared by combining DPPC, POPG, and PA at a ratio of 68:22:9 by weight in chloroform-methanol 3:1. Lipid samples were dried in a DNA 120 speedvac (Thermo Electron, Holbrook, NY) to complete dryness, forming a pellet. The pellet was then dispersed in an aqueous buffer solution (150 mM NaCl, 5 mM $CaCl_2$, 10 mM HEPES, pH 6.9) to the appropriate concentration (0.1 or 1.0 mg/ml), with a final volume of 70–80 μl. Samples were mixed with a pipette 20 times, sonicated with a Fisher model 60 (Hanover Park, IL) probe sonicator for 15 s twice, and then again mixed with a pipette 20 times. This preparation technique was adapted from that of other researchers (18, 35). Infasurf, which contains phospholipids, neutral lipids, and the hydrophobic surfactant proteins B and C, was diluted to the appropriate concentration (0.1 or 1.0 mg/ml) with the above buffer and gently mixed, as recommended by the manufacturer.

Pulsating bubble surfactometer studies. Samples were loaded into a sample chamber with a plastic transfer pipette. Putty was placed on the capillary end of the sample chamber during loading and removed before experiments were run; a similar procedure was previously shown to prevent surfactant leakage (24). The sample chamber was placed into the PBS, and a 0.4-mm radius bubble was formed immediately. Static-bubble adsorption data were collected for 20 min, both with and without adjusting the bubble size.

Dynamic adsorption data were obtained at frequencies of 20 cycles/min until steady state was reached, then at 60 cycles/min for 5 min, 20 cycles/min for 5 min, and 1 cycle/min for 10 min. Experiments were performed both with and without adjusting the bubble size. The order of cycling rate was investigated, and we found that as long as 1 cycle/min did not directly follow 60 cycles/min, there were no differences in data loops (data not shown). For consistency of experiments, we chose the above protocol for all data reported in this paper. In the dynamic experiments, we assumed steady state was attained when the minimum and maximum surface tension remained constant (within 2 dyn/cm), and the shape (slopes and hysteresis) of the surface tension vs. interfacial area loop appeared constant for >2 min. These same criteria were used to determine reproducibility between runs. Each sample was repeated for a total of six times to confirm repeatability of results. Data were collected using both the commercially available PBS software and the image-analysis system. Because the data collection rate at 60 cycles/min was near the temporal resolution of the camera, those data are not presented here. However, the trends observed thus far at 60 cycles/min are consistent with the other data presented here.

RESULTS

All samples were characterized both with and without adjusting the bubble size throughout the run. Although adjusting the bubble size is standard protocol in the field, it is well known that it can affect the adsorption dynamics of the surfactant by introducing "unscheduled" compressions and expansions. Here we present results using both protocols: those with adjusting the bubble size to show how it compares to the standard protocol and those without adjusting the size to give a more accurate assessment of adsorption dynamics.

Adsorption data obtained under static conditions are shown in Fig. 3. In one set of experiments, we maintained the bubble radius at 0.4 mm by manual adjustment (*A–C*), whereas in a second set of experiments we allowed bubble size to drift during data collection (*D–F*). Data were collected for DPPC (*A*, *D*), Infasurf (*B*, *E*), and Tanaka lipids (*C*, *F*), with a sample concentration of 1.0 mg/ml. As reported in other studies, DPPC (4, 35) and Tanaka lipids (1, 23, 26) adsorbed to the interface more slowly than did Infasurf (27) and showed substantially higher surface tensions after 20 min. When the bubble radius was held constant at 0.4 mm, there was very little difference observed between the surface tensions calculated by the original and modified programs, as would be expected. This is due to the spherical shape of the bubble during this static adsorption phase. When the bubble size was not adjusted, the bubble grew during the same period that surfactant was adsorbing to the interface. For example, for the data shown in Fig. 3, *D–F*, the bubble increased in surface area from an original area of 1.7 mm^2 for all samples to 2.7 mm^2 for DPPC, 2.7 mm^2 for Infasurf, and 2.6 mm^2 for Tanaka lipids. This growth in bubble size varied from one run to another and did not seem to depend on the surfactant used. Because the original PBS software was written with the assumption of constant minimum bubble radius, whereas it is actually increasing, the surface tensions obtained using the original PBS software were lower than those obtained by use of the image-analysis system.

Figure 4 shows typical surface tension-interfacial area profiles at different times during cycling, as obtained for the three surfactant preparations at 20 cycles/min and 1.0 mg/ml with bubble size adjusted throughout the run, for DPPC (*A–C*), Infasurf (*D–F*), and Tanaka lipids (*G–I*). Figure 4, *A*, *D*, and *G*, show loops after ~1 min of cycling; *B*, *E*, and *H* show loops after ~5 min of cycling; and *C*, *F*, and *I* show loops at steady state. We should note that at very low surface tensions, such as was obtained for DPPC and Infasurf, the image-analysis system was not always able to fit the shape of the bubble because it varied significantly from that of an ellipse. Therefore, reliable calculations of surface tension and surface area could not be obtained. However, because the pressure drop across the bubble was very low at these time points, it is clear that the surface tension is near zero for these "missing" data points (see Fig. 4, *C–F*).

The dynamic interfacial behavior observed for DPPC is similar to that reported by other investigators (18). Namely, a large degree of compression is required to achieve near-zero surface tension, a high maximum surface tension, and a small extent of loop hysteresis. For Infasurf, we observe near-zero surface tension with a relatively small amount of compression, low maximum surface tension, and a larger extent of hysteresis. These results are consistent with previous studies (27). Finally, the data loops for the Tanaka lipids showed higher minimum and maximum surface tensions than DPPC and Infasurf, as well as a relatively small extent of hysteresis, although slightly more than DPPC. Again, these results compare well with those previously reported by others (1, 23, 26).

However, there are several differences between the shapes of the data loops obtained from the commercial system and our

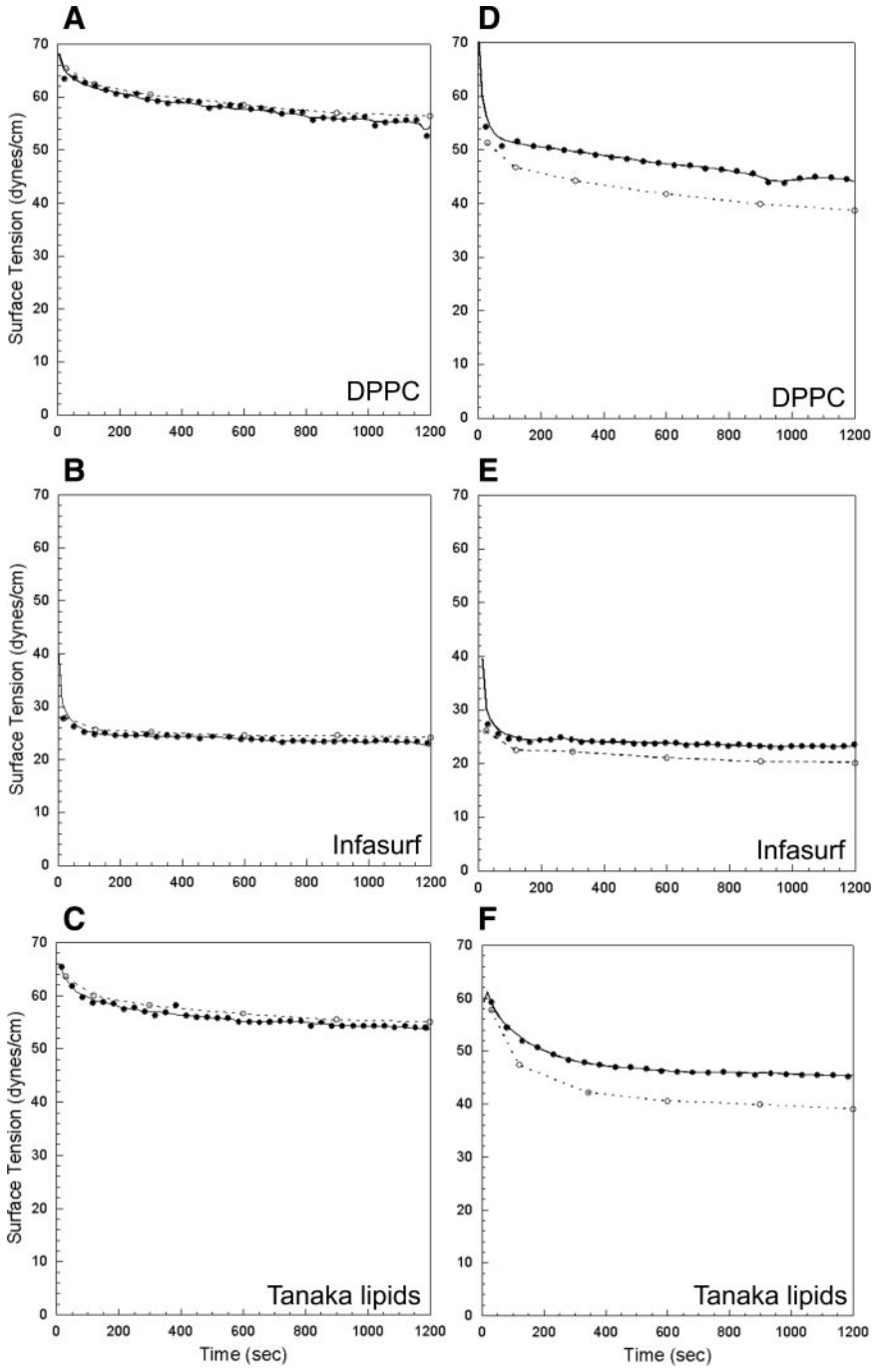

Fig. 3. Surface tension as a function of time for dipalmitoylphosphatidylcholine (DPPC; *A* and *D*), Infasurf (*B* and *E*), and Tanaka lipids (*C* and *F*) at 1.0 mg/ml and 37°C under static-bubble conditions, with adjusting bubble size (*A–C*) and without adjusting bubble size (*D–F*). ●, Data from the new imaging system; ○, data from commercially available software.

modified imaging system. Whereas the minimum surface tensions are similar, the maximum surface tensions calculated by the commercial system are consistently lower than those measured by the modified system. Additionally, we observe significantly decreased hysteresis using the image-analysis system in most of the loops compared with the commercial PBS, as well as differences in the slopes of the curves upon bubble expansion. We focus on examining these and other differences between the commercially available system and the image-analysis system for profiles that have reached a quasi-steady state.

Figure 5 shows the steady-state loops obtained at bulk surfactant concentrations of 0.1 and 1.0 mg/ml, and cycling frequencies of 1 and 20 cycles/min, for DPPC (*A–C*), Infasurf (*D–F*), and Tanaka lipids (*G–I*), with adjustment of bubble size throughout the run. It is clear that the conclusions drawn from the transient loops seen in Fig. 4 are also supported by the data shown in Fig. 5. Namely, the maximum surface tension calculated by the original system is consistently lower than that calculated by the modified system. In many of the loops, the extent of hysteresis seen with the commercially available system is much greater than that seen with the image-analysis system. In some cases (e.g., Figs. 4*B*, 5*A*, and 5*G*), there is virtually no hysteresis detected with the image-analysis system. There is also a significant difference in the slopes of the surface tension-interfacial area curves determined by the de-

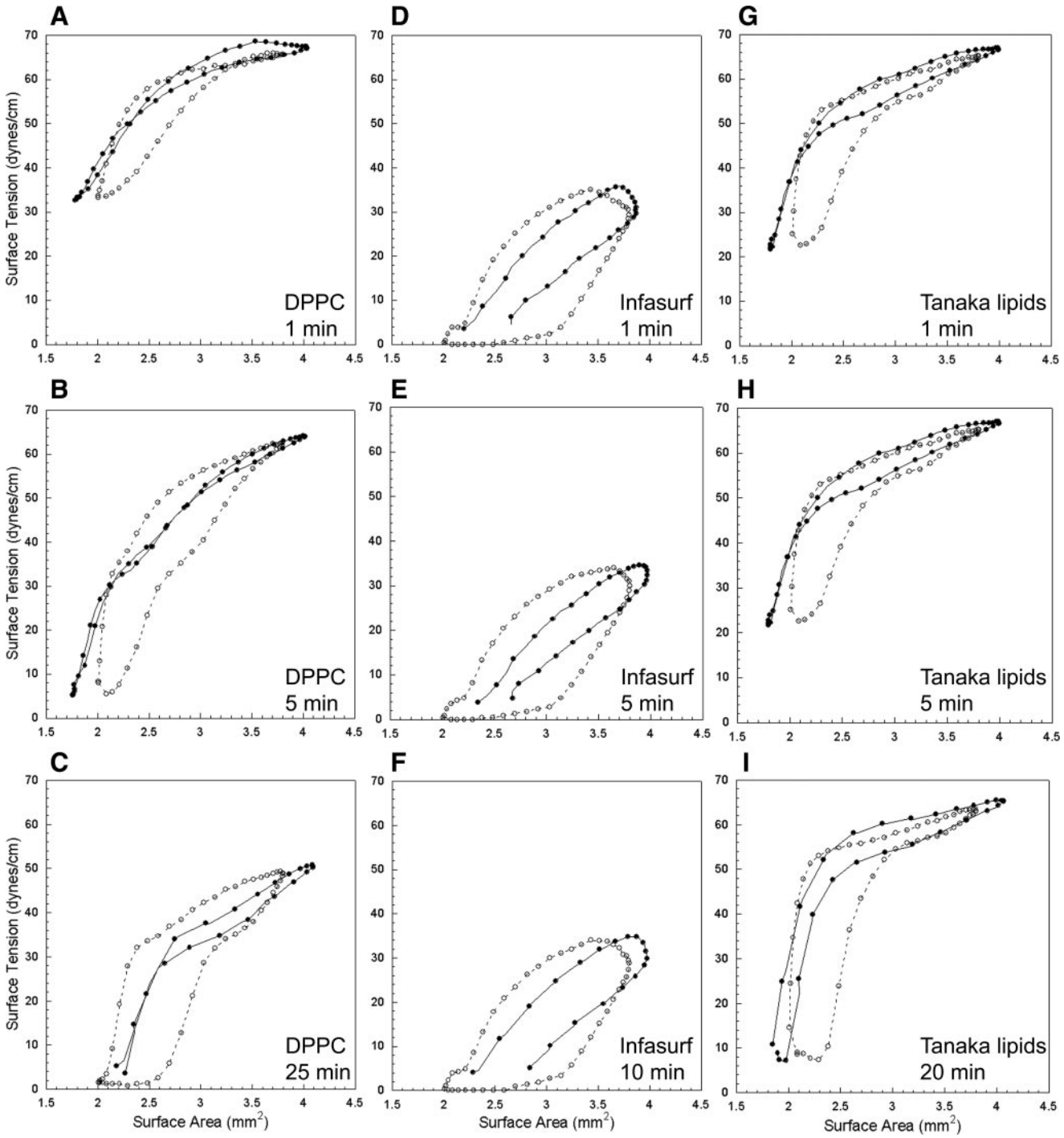

Fig. 4. Surface tension as a function of interfacial area for DPPC (*A–C*), Infasurf (*D–F*), and Tanaka lipids (*G–I*) at 1.0 mg/ml and 37°C with a frequency of 20 cycles/min, at 3 different times after start of cycling. ●, Data from the new imaging system; ○, data from commercially available software. Loop directions are clockwise. Bubble size was adjusted during the run to maintain constant maximum size.

vices, particularly during the initial inflation of the bubble. Although the commercially available device shows a very high slope, as has been noted in previous studies (18, 20, 21), this slope is usually significantly lower when data are acquired with the image-analysis system (e.g., Figs. 4*G* and 5*D*).

We have determined several reasons why these errors may occur with the commercial system. First, we observe a difference in the cyclic change in surface area for each cycle. The original software assumes the compression ratio to be 47.4% of mean bubble surface area, whereas that detected by the image-analysis system ranged from ~50 to 58%, depending on bubble size and cycling rate. Because of these differences between the true and assumed bubble size, significant differences in the shapes of the surface tension-interfacial area profiles are observed between the two systems. This is the cause for the lower maximum surface tension obtained from

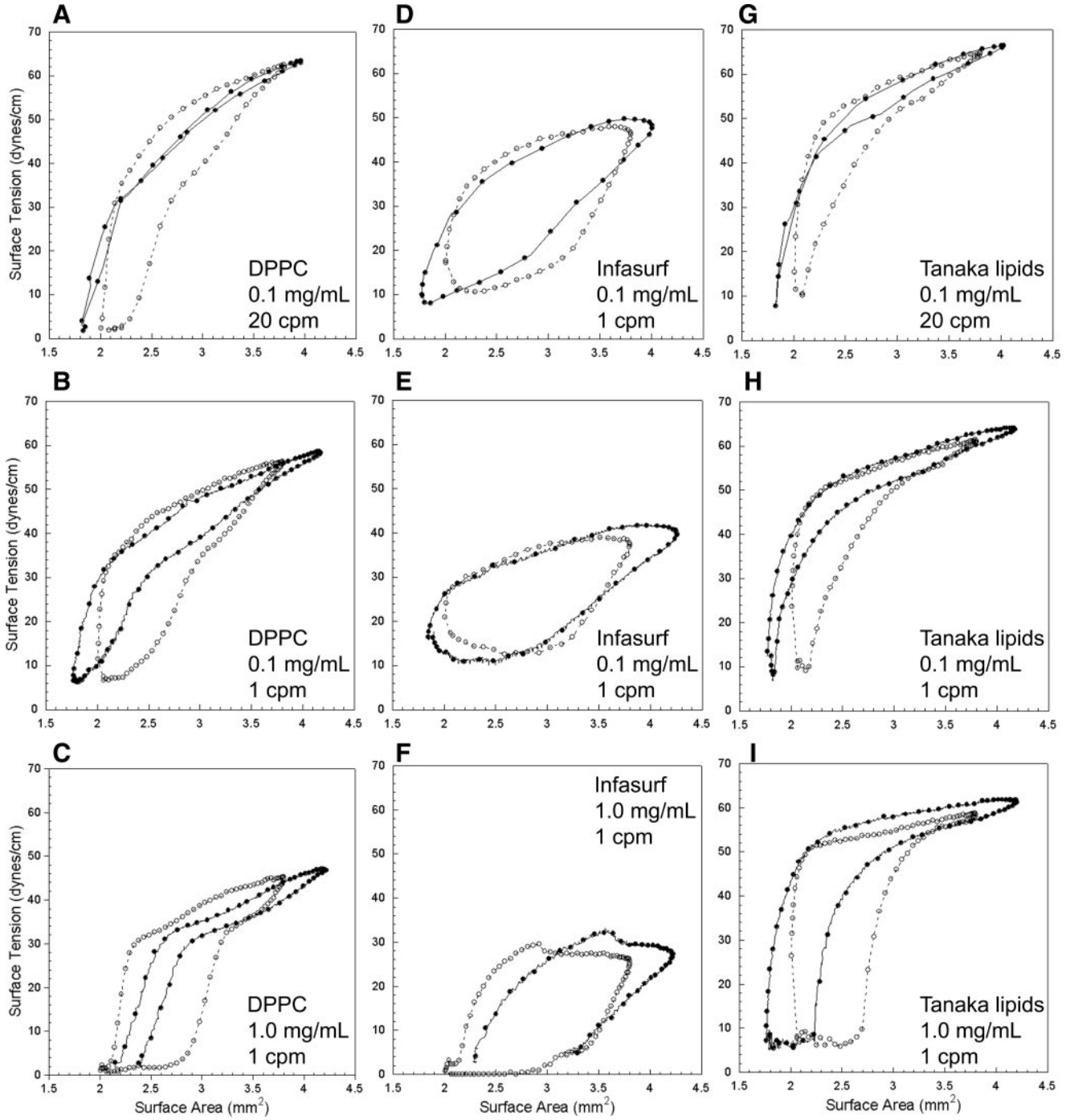

Fig. 5. Steady-state surface tension as a function of interfacial area for DPPC (*A–C*), Infasurf (*D–F*), and Tanaka lipids (*G–I*) at 0.1 mg/ml (*A*, *B*, *D*, *E*, *G*, *H*) and 1.0 mg/ml (*C*, *F*, *I*) and 37°C at frequencies of 20 cycles/min (cpm) (*A*, *D*, *G*) and 1 cycle/min (*B*, *C*, *E*, *F*, *H*, *I*). ●, Data from the new imaging system; ○, data from commercially available software. Loop directions are clockwise. Bubble size was adjusted during the run to maintain constant maximum size.

the original system, because the bubble is increasing to a larger maximum surface area than is assumed.

Another source of error is the sinusoidal change in cyclic volume assumed in the software of the commercially available system. The image-analysis system shows that the volume does not change in exactly a sinusoidal fashion, but rather the peaks and troughs are somewhat flatter than would be the case for a true sinusoid (data not shown). This can cause the commercially available device to show an apparent increase in surface tension before the surface area has reached its minimum value, unlike most of the data measured by the image-analysis system.

We have also observed a discrepancy between the bubble cycling frequencies as measured by the image-analysis system compared with that detected by the commercially available PBS software. When the unit is running at a frequency of 20 cycles/min, the image-analysis system measures the correct frequency. However, the commercially available device detects a somewhat higher frequency of 20.68 cycles/min. According

to the manufacturer, this may be due to a slow chip in the device, leading to inadequate processor speed involved in data storage. A similar discrepancy was seen at 1 cycle/min, with the commercially available device detecting a frequency of 1.04 cycles/min. Although these differences are small and do not generate significant errors in terms of measured surface tension or shapes of the hysteresis loops, they do lead to a time-dependent phase difference between the real data (as recorded by our imaging system) and the data as recorded by the PBS software.

Finally, there is the issue of bubble size drift that occurs during the time course of an experiment. Although it is common practice in the use of the commercial device to constantly adjust the bubble size throughout the run, this is tedious and inaccurate and can lead to changes in the adsorption kinetics. Figure 6 shows hysteresis loops for 1.0 mg/ml DPPC at 20 cycles/min without adjusting bubble size after 1 min (*A*), 5 min (*B*), and at equilibration, or 35 min (*C*) of cycling. The upward drift in surface area is readily apparent in Fig. 6 for the data acquired by the imaging system. The bubble begins at a maximum surface area of 4.0 mm^2; however, image analysis reveals that, for these particular runs, the maximum surface area of the DPPC bubble grew to 4.3 mm^2 over 35 min (Fig. 4*C*). This leads to a progressively larger error in the maximum surface tension, as measured by the commercially available system.

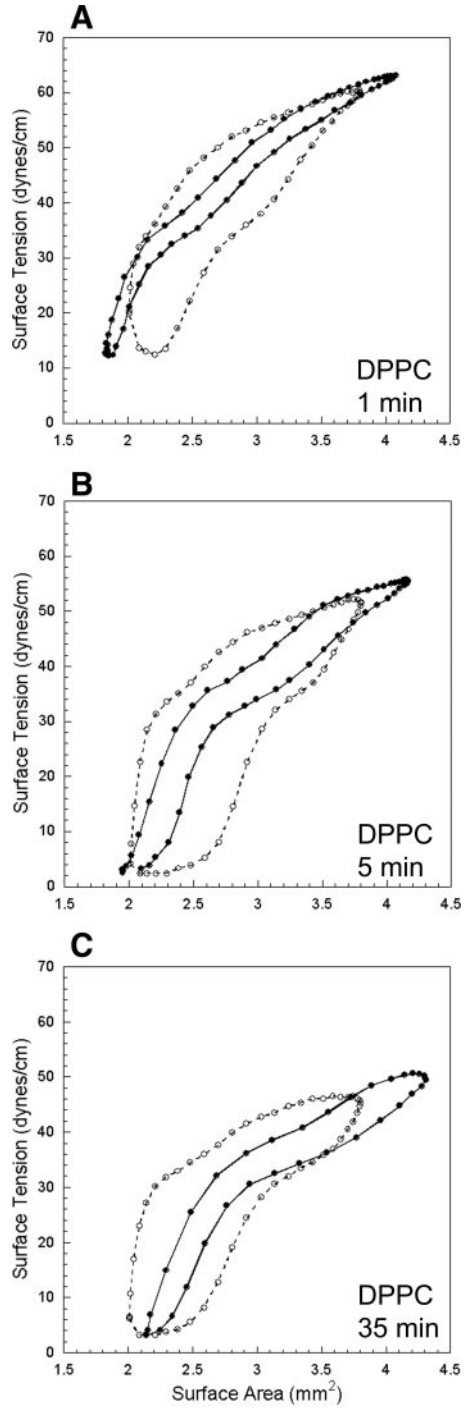

Fig. 6. Steady-state surface tension as a function of interfacial area for DPPC at 1.0 mg/ml, 37°C, and 20 cycles/min, without adjusting bubble size, after 1 min (*A*), 5 min (*B*), and 35 min (*C*) of cycling. ●, Data from the new imaging system; ○, data from commercially available software. Loop directions are clockwise.

DISCUSSION

The PBS allows for characterization of the dynamic behavior of surfactant preparations at physiological frequencies. As normally used, the PBS allows the minimum and maximum surface tension of a preparation to be determined at different pulsation frequencies (9). Another instrument used for the characterization of surfactants is the captive bubble surfactometer (CBS), which is a leak-proof surfactometer that utilizes image analysis to determine the dynamic surface tension behavior (28). Although the CBS has some distinct advantages over the PBS, such as minimizing surfactant leakage and thereby better characterizing the dynamic behavior of surfactants, particularly those with high surface activity (24, 28), there are also some disadvantages. In particular, there are some difficulties with its use: large quantities of surfactant are necessary to load the system; experiments are time consuming; and the data analysis can be quite complex and therefore too time consuming to be done in real time (24). Although the limitations of the PBS have been noted in several reports (5, 8, 14, 24), the relative ease of working with this system, compared with other systems, as well as its commercial availability, have led to its continued use.

However, the commercially available PBS system also has several distinct problems, including the assumptions made in its software that the bubble is a sphere with constant maximum and minimum radii (0.55 and 0.4 mm, respectively), and that the cyclic change in bubble volume is sinusoidal. Although the device is generally able to provide accurate values for the minimum surface tension when the bubble size is adjusted throughout the run, other data that can be obtained from the shape of the surface tension-interfacial area loop are inaccurate. In particular, parameters such as the extent of loop hysteresis, surface film elasticity, dynamic respreading, and compression needed to reach minimum surface tension all depend strongly on the shape of the surface tension-interfacial area loop. Therefore, to obtain accurate data from this system, the bubble size and shape need to be accurately and dynamically determined.

By enhancing the PBS with an imaging and data-acquisition system that sends images and voltage signals from the device

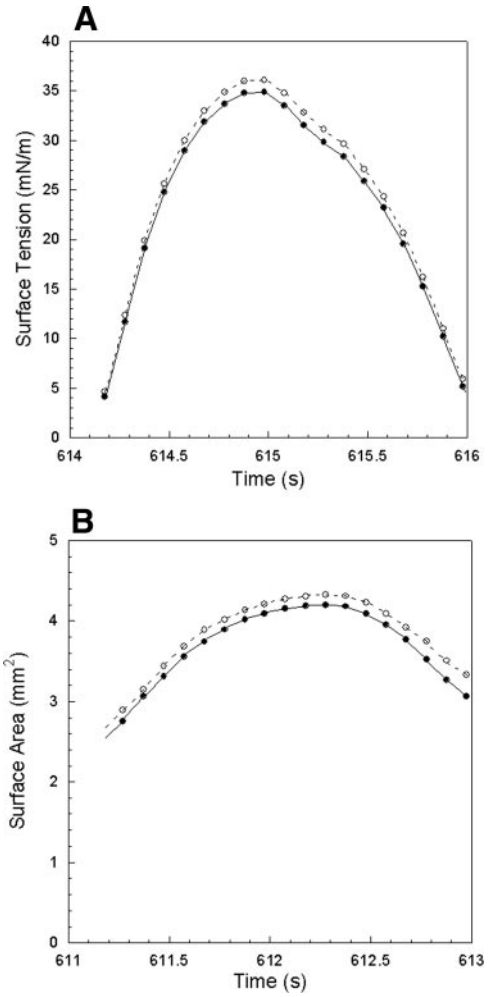

Fig. 7. Comparison of spherical vs. ellipsoidal shape assumption for DPPC at 1.0 mg/ml, 37°C, and 20 cycles/min. *A*: steady-state surface tension as a function of time. *B*: surface area (capillary tube area not corrected for) as a function of time. ●, Data assuming an ellipsoid; ○, data assuming a sphere. Loop directions are clockwise.

to a personal computer running in-house data-reduction software, we are able to dynamically and accurately track bubble size and shape, as well as chamber pressure, and thereby surface tension. Because we are able to correctly determine the bubble shape, the bubble can be fitted to an ellipse rather than assuming that the bubble is spherical, as is done with the commercial unit. Figure 7 shows a comparison of surface tension (*A*) and surface area (*B*) as a function of time for the same bubble, assuming either a spherical or ellipsoidal shape. As expected, at high surface tensions when the bubble is nearly spherical, only ~3% error in both surface tension and surface area is introduced by assuming a spherical vs. ellipsoidal bubble shape. However, at low surface tensions there is ~15% error in the calculated surface tension and ~10% error in the calculated surface area introduced by assuming the bubble is spherical. The modified system is also able to correct the surface area by accounting for the area of the capillary tube to which the bubble is attached, thereby including only the surface area of the bubble available to surfactant. The difference in surface areas with and without this correction ranges from 7 to 12%, depending on bubble size. Finally, we corrected the calculated surface tension for the effects of gravity on hydrostatic pressure.

In addition, the modified system is able to detect the actual compression ratio, which typically varies from that assumed by the original system. As can be seen in Figs. 4 and 5, the compression ratio is distinctly different from that assumed by the PBS, likely leading to many differences in the shape of the loop. Finally, this approach allows for direct visual assessment of whether leakage of surfactant into the capillary is occurring during a run. If leakage is detected, the data can be rejected. The results show that, without these corrections, significant errors can occur in the characterization of a surfactant preparation.

Typically, results from the PBS are presented in table form: minimum and maximum surface tension at given times after the beginning of pulsation. However, there is a great deal of information that can be gained from the examination of the interfacial area-surface tension loops. Comparison of these loops with analytical models can be used to determine biophysical parameters characterizing surfactant function (18, 20–22). Interestingly, previous comparisons of model predictions with results from the commercially available PBS identified differences that were attributed to deficiencies in the models (18, 21, 22). In particular, the models predicted less hysteresis, with the hysteresis depending more strongly on frequency than was seen in the data from the commercially available PBS. Furthermore, the rapid increase in surface tension at the beginning of bubble inflation that was seen using the commercially available PBS could not be reproduced by model predictions.

It is exciting to find that these are precisely the differences between the loops as seen when using the image-analysis system and those seen when using the commercially available unit, with the model predictions agreeing much more closely with the former. Figures 4 and 5 reveal less hysteresis and also a much stronger dependence of hysteresis on cycling frequency in the data from the image-analysis system than was seen using the commercially available unit. Nearly all of the figures show that the image-analysis system has a much slower increase in surface tension at the start of bubble inflation than is seen using the commercially available system. This high rate of increase in surface tension seen with the commercially available system has been commented on in other studies (18, 22) and likely occurs because of errors in assumed size and shape of the bubble as determined by PBS software at very low surface area. Although the bubble is still decreasing in surface area, the commercially available system assumes it is already increasing.

It is also of note that the data from the image-analysis system compare well with dynamic measurements of the behavior of lung surfactant in a CBS (29). Specifically, at 50% film area compression, minimal hysteresis was observed with the CBS, and the initial slope upon film expansion was similar to that seen in this study. This is in contrast to the findings obtained by use of the commercially available PBS. All of these findings not only strongly suggest that these models give a more accurate portrayal of surfactant biophysical function than previously realized, but also lend further support to the results of the present study.

The modified PBS system, with image- and data-analysis capabilities, allows for more accurate characterization of lung surfactant preparations. However, there are still several weak-

nesses of the new system. Although we are able to account for ellipsoidal bubble shape rather than assuming a sphere, at near-zero surface tensions the bubble becomes flattened, sometimes beginning to wrap around the capillary tube, and thus is no longer ellipsoidal in shape. The modified program is therefore not able to fit the bubble shape accurately in this regime. In addition, with the camera we are currently using, we are only able to transfer images at a rate of 60 per second. This is not sufficient for obtaining accurate data at 60 cycles/min, causing a lag in the image with regard to the pressure measurement. We plan to remedy this issue by acquiring a camera with a higher data-transfer rate.

Whereas the original PBS system is able to accurately determine the minimum surface tension, the maximum surface tension and the shapes of the interfacial area-surface tension loops that it reports are inaccurate. Accurate determinations of these loop shapes are especially important for determining the rate of increase of surface tension during inflation. It has been suggested that uniform inflation and stability of the lung depend strongly on the rate of increase of surface tension during lung inflation (10, 11, 30). The new image-analysis system allows dynamic determination of both bubble shape and size, which necessarily leads to a more accurate determination of parameters that characterize the inflation-deflation loops.

Use of the image-analysis system identified several problems associated with the use of the original PBS system. The determination of surface tension relied on a number of calculated quantities, particularly the bubble compression ratio, sinusoidal volumetric changes, cycling frequency, and bubble size and shape. Of these, errors in bubble compression ratio and the sinusoidal assumption led to the most significant errors in the surface tension-interfacial area profiles. The loops that we obtain with the modified system better match model predictions. This modified device will allow for rapid and accurate determination of biophysical parameters that characterize potential lung surfactant replacement preparations.

GRANTS

We acknowledge support from the National Institutes of Health (P01-HL33009, M. Johnson and 1R01HL67984-01, A. E. Barron), start-up funds from Northwestern University, Office of the Vice President and the McCormick School of Engineering (M. Johnson), and from the National Science Foundation (BES-0101195 and BES-9870386, A. E. Barron).

REFERENCES

1. **Amirkhanian JD, Bruni R, Waring AJ, Navar C, and Taeusch HW.** Full-length synthetic surfactant proteins, SP-B and SP-C, reduce surfactant inactivation by serum. *Biochim Biophys Acta* 1168: 315–320, 1993.
2. **Beyer WH.** *CRC Standard Mathematical Tables*. Boca Raton, FL: CRC, 1987.
3. **Bruni R, Hernandez-Juviel JM, Tanoviceanu R, and Walther FJ.** Synthetic mimics of surfactant proteins B and C: in vitro surface activity and effects on lung compliance in two animal models of surfactant deficiency. *Mol Genet Metab* 63: 116–125, 1998.
4. **Chang CH, Coltharp KA, Park SY, and Franses EI.** Surface tension measurements with the pulsating bubble method. *Colloid Surf A Physicochem Eng Asp* 114: 185–197, 1996.
5. **Chang CH and Franses EI.** An analysis of the factors affecting dynamic tension measurements with the pulsating bubble surfactometer. *J Colloid Interface Sci* 164: 107–113, 1994.
6. **Crane JM and Hall SB.** Rapid compression transforms interfacial monolayers of pulmonary surfactant. *Biophys J* 80: 1863–1872, 2001.
7. **Diemel RV, Snel MME, van Golde LMG, Putz G, Haagsman HP, and Batenburg JJ.** Effects of cholesterol on surface activity and surface topography of spread surfactant films. *Biochemistry* 41: 15007–15016, 2002.
8. **Enhorning G.** Pulmonary surfactant function studied with the pulsating bubble surfactometer (PBS) and the capillary surfactometer (CS). *Comp Biochem Physiol A* 129: 221–226, 2001.
9. **Enhorning G.** Pulsating bubble technique for evaluating pulmonary surfactant. *J Appl Physiol* 43: 198–203, 1977.
10. **Fung YC.** Does surface-tension make lung inherently unstable. *Circ Res* 37: 497–502, 1975.
11. **Fung YC.** Stress, deformation, and atelectasis of lung. *Circ Res* 37: 481–496, 1975.
12. **Graves DJ, Merrill EW, Smith KA, and Gilliland ER.** Cinematographic method for measurement of rapidly changing surface tension-area functions. *J Colloid Interface Sci* 37: 303–311, 1971.
13. **Griese M.** Pulmonary surfactant in health and human lung diseases: state of the art. *Eur Respir J* 13: 1455–1476, 1999.
14. **Hall SB, Bermel MS, Ko YT, Palmer HJ, Enhorning G, and Notter RH.** Approximations in the measurement of surface tension on the oscillating bubble surfactometer. *J Appl Physiol* 75: 468–477, 1993.
15. **Halliday HL.** Controversies: synthetic or natural surfactant. The case for natural surfactant. *J Perinat Med* 24: 417–426, 1996.
16. **Hennes HM, Lee MB, Rimm AA, and Shapiro DL.** Surfactant replacement therapy in respiratory-distress syndrome. Metaanalysis of clinical trials of single-dose surfactant extracts. *Am J Dis Child* 145: 102–104, 1991.
17. **Hiemenz PC and Rajagopalan R.** *Principles of Colloid and Surface Chemistry*. New York: Dekker, 1997.
18. **Ingenito EP, Morris LMJ, Espinosa FF, Kamm RD, and Johnson M.** Biophysical characterization and modeling of lung surfactant components. *J Appl Physiol* 86: 1702–1714, 1999.
19. **Johansson J, Gustafsson M, Palmblad M, Zaltash S, Robertson B, and Curstedt T.** Synthetic surfactant protein analogues. *Biol Neonate* 74: 9–14, 1998.
20. **Krueger MA and Gaver DP.** A theoretical model of pulmonary surfactant multilayer collapse under oscillating area conditions. *J Colloid Interface Sci* 229: 353–364, 2000.
21. **Morris J, Ingenito EP, Mark L, Kamm RD, and Johnson M.** Dynamic behavior of lung surfactant. *Trans ASME* 123: 106–113, 2001.
22. **Otis DR, Ingenito EP, Kamm RD, and Johnson M.** Dynamic surface tension of surfactant TA: experiments and theory. *J Appl Physiol* 77: 2681–2688, 1994.
23. **Otsubo E and Takei T.** Characterization of the surface activity of a synthetic surfactant with albumin. *Biol Pharm Bull* 25: 1519–1523, 2002.
24. **Putz G, Goerke J, Taeusch HW, and Clements JA.** Comparison of captive and pulsating bubble surfactometers with use of lung surfactants. *J Appl Physiol* 76: 1425–1431, 1994.
25. **Revak SD, Merritt TA, Cochrane CG, Heldt GP, Alberts MS, Anderson DW, and Kheiter A.** Efficacy of synthetic peptide-containing surfactant in the treatment of respiratory distress syndrome in preterm infant rhesus monkeys. *Pediatr Res* 39: 715–724, 1996.
26. **Sarin VK, Gupta S, Leung TK, Taylor VE, Ohning BL, Whitsett JA, and Fox JL.** Biophysical and biological-activity of a synthetic 8.7-kDa hydrophobic pulmonary surfactant protein SP-B. *Proc Natl Acad Sci USA* 87: 2633–2637, 1990.
27. **Scarpelli EM, David E, Cordova M, and Mautone AJ.** Surface tension of therapeutic surfactants (Exosurf Neonatal, Infasurf, and Survanta) as evaluated by standard methods and criteria. *Am J Perinatol* 9: 414–419, 1992.
28. **Schürch S, Bachofen H, Goerke J, and Possmayer F.** A captive bubble method reproduces the in situ behavior of lung surfactant monolayers. *J Appl Physiol* 67: 2389–2396, 1989.
29. **Schurch S, Schurch D, Curstedt T, and Robertson B.** Surface-activity of lipid extract surfactant in relation to film area compression and collapse. *J Appl Physiol* 77: 974–986, 1994.
30. **Stamenovic D and Smith JC.** Surface forces in lungs. II. Microstructural mechanics and lung stability. *J Appl Physiol* 60: 1351–1357, 1986.
31. **Suresh GK and Soll RF.** Exogenous surfactant therapy in newborn infants. *Ann Acad Med Singapore* 32: 335–345, 2003.
32. **Tanaka Y, Takei T, Aiba T, Masuda K, Kiuchi A, and Fujiwara T.** Development of synthetic lung surfactants. *J Lipid Res* 27: 475–485, 1986.
33. **Veldhuizen EJA, Batenburg JJ, van Golde LM, and Haagsman HP.** The role of surfactant proteins in DPPC enrichment of surface films. *Biophys J* 79: 3164–3171, 2000.

34. **Waring A, Taeusch HW, Bruni R, Amirkhanian J, Fan BCR, Stevens R, and Young J.** Synthetic amphipathic sequences of surfactant protein B mimic several physiochemical and in vivo properties of native pulmonary surfactant proteins. *Pept Res* 2: 308–313, 1989.
35. **Wen X and Franses EI.** Role of subsurface particulates on the dynamic adsorption of dipalmitoylphosphatidylcholine at the air/water interface. *Langmuir* 17: 3194–3201, 2001.
36. **Wu CW and Barron AE.** Biomimetic lung surfactant replacements. In: *Biomimetic Materials and Design: Interactive Biointerfacial Strategies, Tissue Engineering, and Drug Delivery*, edited by Dillow AK and Lowman A. New York: Dekker, 2002, p. 565–633.
37. **Wu CW, Seurynck SL, Lee KYC, and Barron AE.** Helical peptoid mimics of lung surfactant protein C. *Chem Biol* 10: 1057–1063, 2003.